Measurement of metastable He-*(2(3)S(1)) density in dielectric barrier discharges with two different configurations operating at around atmospheric pressure

AUTHOR(S):

Tachibana, K; Kishimoto, Y; Sakai, O

JOURNAL OF APPLIED PHYSICS **97**, 123301 (2005)

Measurement of metastable $He^*(2^3S_1)$ density in dielectric barrier discharges with two different configurations operating at around atmospheric pressure

K. Tachibana,[a] Y. Kishimoto, and O. Sakai
Department of Electronic Science and Engineering, Kyoto University, Kyoto-Daigaku Katsura, Nishikyo-ku, Kyoto 615-8510, Japan

(Received 27 January 2005; accepted 4 April 2005; published online 16 June 2005)

We have measured the density of metastable He atoms in the lowest triplet state (2^3S_1) with a diode-laser absorption spectroscopic technique in atmospheric pressure plasmas produced by dielectric barrier discharge schemes. Two different types of electrode configuration are employed: one is a conventional parallel-plate system and the other is a microdischarge integrated system with stacked metal-mesh electrodes covered by insulating films. We have analyzed the pressure-broadened spectral line corresponding to the $2^3S_1 \rightarrow 2^3P_J$ ($J=0$–2) transition to derive the broadening coefficient and to calibrate absolute densities. The measured density ranges from 10^{11} to 10^{12} cm^{-3}, but the values in the mesh-type system are larger than those in the parallel-plate system by about one order of magnitude. The density, however, depends strongly on the gas flow rate, showing the influence of quenching by the Penning-ionization process with impurities. Those behaviors are consistent with the variation of the electron density estimated by millimeter-wave transmittance measurement. © *2005 American Institute of Physics*. [DOI: 10.1063/1.1922581]

I. INTRODUCTION

Recently, atmospheric pressure discharge has attracted much interest due to its potential applicability to various surface-treatment techniques.[1–3] In many cases, dielectric barrier discharge (DBD) schemes with electrodes covered by insulating materials are used to realize uniform-looking discharge, which is sometimes called atmospheric pressure glow discharge (APGD).[3–5] However, there is much contention as to whether it is a glow discharge in the usual sense or only looks like one. In recent publications, Massines and co-workers[6,7] and Golubovskii *et al.*[8,9] have concluded that APGD is obtained in He as the glow discharge mode, where a potential distribution corresponding to cathode dark space, negative glow, etc., are seen as in a conventional glow discharge. However, in N_2 APGD can be realized only in the Townsend discharge mode, where no such potential distribution can be clearly recognized.[6–9]

In any case, it is important to investigate the difference by employing internal plasma parameters such as the densities of electrons, ions and excited species. For this purpose, we have started diagnostics of those parameters as the first step. Here, we use two different DBD structures: one is a conventional parallel-plate system in which two metal plate electrodes are covered by alumina (Al_2O_3) plates placed in parallel with a gas gap of a few millimeter;[10] the other is a microdischarge integrated system with stacked metal-mesh electrodes coated with Al_2O_3 thick films.[11] With these plasma sources the density of He metastable atoms in the first excited 2^3S_1 state [designated as $He^*(2^3S_1)$ hereafter] is measured by laser absorption spectroscopy (LAS) using a tunable diode laser as the light source.[12] On the way to deriving the absolute value, the spectral line profile is analyzed and the pressure-broadening coefficient is derived experimentally. The effect of impurities on the density of $He^*(2^3S_1)$ atoms is also studied systematically by changing the gas flow rate. In addition, we estimate the electron density in those sources with a millimeter-wave transmittance technique. Based on these results, we discuss the behaviors of the metastable atom density and the difference in those two plasma sources.

II. EXPERIMENTAL SETUP AND PROCEDURES

The plasma sources of two different types are shown in Fig. 1, the details of which have been described in our previous papers.[10,11] In short, as Fig. 1(a) shows, the parallel-plate system has two 60 mm in diameter metal plate electrodes covered by square ceramic plates 80×80 mm^2 in area and 0.7 mm thick. These pairs are separated by glass spacers 3 mm thick and 25 mm in width, with a 10-mm-wide gas-feed space on one side. Therefore, the effective electrode area becomes 18 cm^2. A bipolar pulse power source was used and the square-wave output was stepped up by a high-voltage transformer, so that the output wave form was composed of an impulse peak V_0 followed by a ringing tail with the first peak V_1. Those two parameters, V_0 and V_1, characterizing the wave form were important for realizing APGD in N_2 gas and even in air, as described previously.[10] In He gas, however, APGD was obtained easily without any critical region in those parameters. The frequency ($1/T$) was set typically at 5 kHz. In the mesh-type system shown in Fig. 1(b), the unit microdischarge had an effective opening area of 600×1550 μm^2 arranged in a pitch of 1200×2500 μm^2. The total electrode area was 50 mm in diameter. The system was connected to a bipolar pulse power supply, which pro-

[a]Electronic mail: tatibana@kuee.kyoto-u.ac.jp

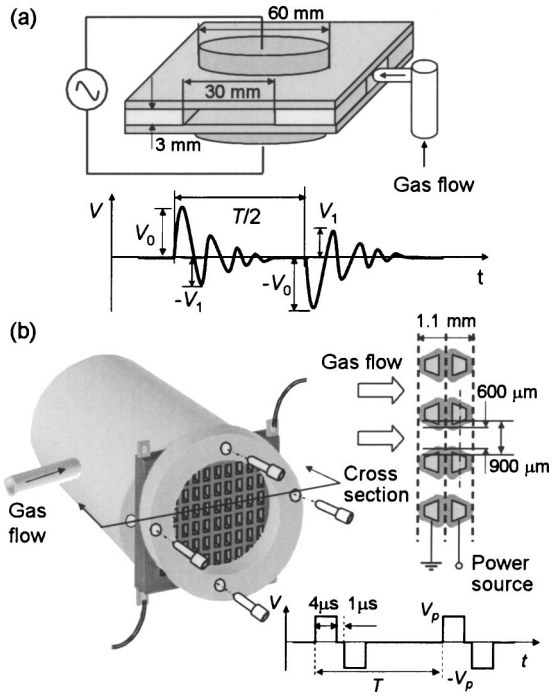

FIG. 1. Schematics of (a) the parallel-plate system and (b) the mesh-electrode system and the corresponding driving voltage wave forms.

vided a pair of positive and negative pulses, $+V_p$ and $-V_p$, of 4 μs width with an intermittent time of 1 μs at a repetition frequency $(1/T)$ of 5 kHz.

Each electrode assembly was placed in a vaccum chamber and pumped by a roughing pump to a base pressure of approximately 10^{-3} Torr. In the parallel-plate system the gas flow was conducted from the side to flow through the channel formed by the gas gap, while in the mesh-type system the gas was fed from the back side through the mesh structure perpendicularly. The gas flow was regulated up to two standard liters per min (SLM).

We used a commercial diode-laser system for the LAS measurements. The wavelength was tuned to the $(2^3S_1 \rightarrow 2^3P_J, J=0,1,2)$ transition of He atoms at around 1082 nm. In most of the present measurements, we selected two components with $J=1$ and 2 due to the higher absorption coefficients. However, as the pressure is increased, those components overlapped with each other due to the pressure-broadening effect. The overlapped shape was expressed by a superposition of two Voigt profiles with an intensity ratio of 5:3 and a separation of 2.3 GHz. The Gaussian (Doppler broadening) component of the Voigt profile $\Delta\nu_D$ (full width at half maximum, FWHM) is taken to be 1.72 GHz at the assumed gas temperature of 300 K, while the Lorenzian (pressure-broadening) component $\Delta\nu_L$ (FWHM) was varied to fit the measured profile. The absolute density of $He^*(2^3S_1)$ atoms N_m was derived from the transmittance I/I_0 by integrating the absorption coefficient $k_{if}(\nu)$ of one component, say the transition of $2^3S_1 \rightarrow 2^3P_2$ with the largest absorption, over the frequency ν as follows:

$$I = I_0 \exp[-k_{if}(\nu)L], \tag{1}$$

$$N_m = \frac{8\pi g_i}{\lambda_0^2 g_f A_{fi}} \int k_{if}(\nu) d\nu, \tag{2}$$

where I_0 and I are the incident and transmitted laser intensities, L is the absorption length, λ_0 is the wavelength (=1083 nm), g_i(=3), and g_f(=5) are the statistical weights of the lower i and upper f states, and A_{fi} is the transition probability $(=1.022\times10^7\ s^{-1})$.

Measurements of $He^*(2^3S_1)$ density in the parallel-plate system were carried out by passing the diode-laser beam through the center of the electrode configuration at the height of the mid gap. Therefore, the absorption length L was taken to be equal to the electrode diameter for the derivation of $k_{if}(\nu)$. Measurements in the mesh-type system were performed in two different ways. First, the laser beam was passed through the center axis of one of the microdischarges perpendicularly to the mesh electrode. Second, the beam was aligned parallel to the mesh electrode assembly, and the distance from the electrode surface was changed to reveal the spatial distribution.

To estimate the electron density n_e, we employed a millimeter-wave transmission technique.[13] The millimeter-wave source was a combination of a synthesized sweep signal generator and a harmonic source module, with an output frequency range from 50 to 75 GHz. In the mesh-type system, the electrode assembly was placed normal to the propagation direction and the shorter length of the opening hole was set parallel to the electric vector of the TE_{01} mode of millimeter waves in order to provide greater transmittance. Even though the opening size was smaller than the wavelength, we obtained a transmittance level of more than 30% across the frequency range. In the parallel-plate system the direction of the electrode gap was taken parallel to the electric vector of millimeter waves for the same reason as above. However, because of the greater length through a narrow gap, the transmittance was about 10%, though this was good enough to observe the attenuation by plasma. Metal plate apertures with square holes corresponding to the cross section of the discharge gap were placed in front of the antennas on both sides to avoid the detoured transmittance. The transmittance characteristics were analyzed under a simple assumption of slab-shaped plasma of a certain thickness corresponding to each absorption length.[13,14]

Typical examples of the signals observed in the parallel-plate and metal-mesh systems for the LAS and the millimeter-wave transmission measurements are shown in Figs. 2(a) and 2(b), respectively, together with the wave forms of the applied voltage and the discharge current. Here, the millimeter-wave transmittance signals taken at 55 GHz (hereafter this frequency is used throughout the measurements) are amplified three times for a better visibility. The original current wave form is a superposition of the conduction current and the displacement current. Therefore, the displacement current component was estimated from the derivative of the voltage wave form and substracted from the measured current to yield the conduction current component in each case.

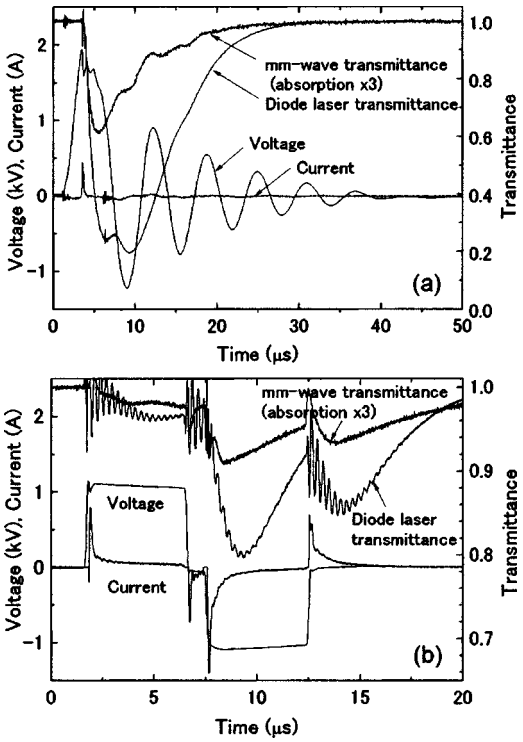

FIG. 2. Examples of wave forms of LAS signals and millimeter-wave transmission signals in (a) the parallel-plate system and (b) the mesh-electrode system, together with wave forms of applied voltage and discharge current.

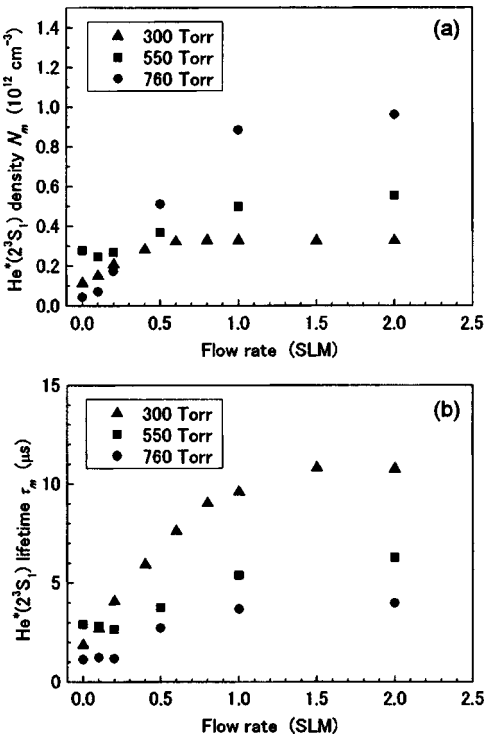

FIG. 4. (a) Density of $He^*(2^3S_1)$ atoms and (b) their lifetime in the afterglow measured in the parallel-plate system as a function of the gas flow rate at three different pressures.

III. RESULTS

A. Pressure broadening of the 1083-nm line

Figure 3(a) shows examples of the absorption line profile measured in the parallel-plate system and the fitted result with the superposed Voigt profile. It can be seen that at 760 Torr the Lorenzian component $\Delta\nu_L$ becomes as large as 13.6 GHz in comparison to the Doppler component $\Delta\nu_D$ of 1.72 GHz. The variation of $\Delta\nu_L$ with the pressure p is shown in Fig. 3(b). Since the pressure dependence is almost linear, we can derive the pressure-broadening coefficient as 18.5 MHz/Torr for the full width at half maximum (FWHM). There is only a theoretical report on the pressure broadening of the 1083-nm line in which the temperature dependence is investigated precisely.[15] The reported value at 300 K is 24.14 MHz/Torr when it is converted into FWHM. Our experimental value is smaller than this theoretical value by about 30%. If we assume a gas temperature of 400 K, the theoretical value drops to 19.88 MHz and the discrepancy with our experimental value becomes much smaller. In the measurement, we kept operating the discharge for about 1 h, so that the gas temperature might increase by 100 K or so. In any case, if the theoretical temperature dependence is reliable, it can provide us a useful method to estimate the gas temperature in active discharges.

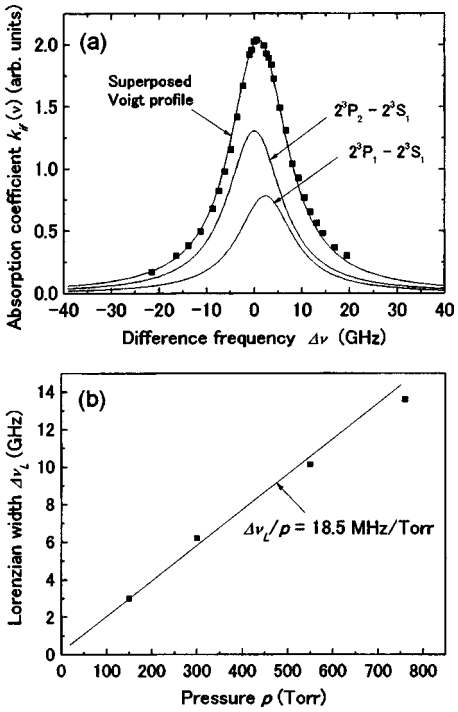

FIG. 3. (a) Pressure-broadened absorption line profile of the $2^3P_{1,2}$-2^3S_1 transitions measured at 1 atm fitted with the superposition of two Voigt profiles, and (b) pressure dependence of the Lorenzian component (FWHM).

B. Metastable density in the parallel-plate system

Figure 4(a) shows the measured values of the $He^*(2^3S_1)$ density N_m in the parallel-plate system as a function of the gas flow rate at several different pressures. The values of V_0 at 300, 550, and 760 Torr were 1.2, 1.5, and 1.8 kV, respectively. It can be seen that at each pressure the density increases with the gas flow rate and then tends to saturate, suggesting the possibility that the impurity level decreases with the gas flow. To observe the mechanism in detail we measured the decay rate γ_m of the density in the afterglow

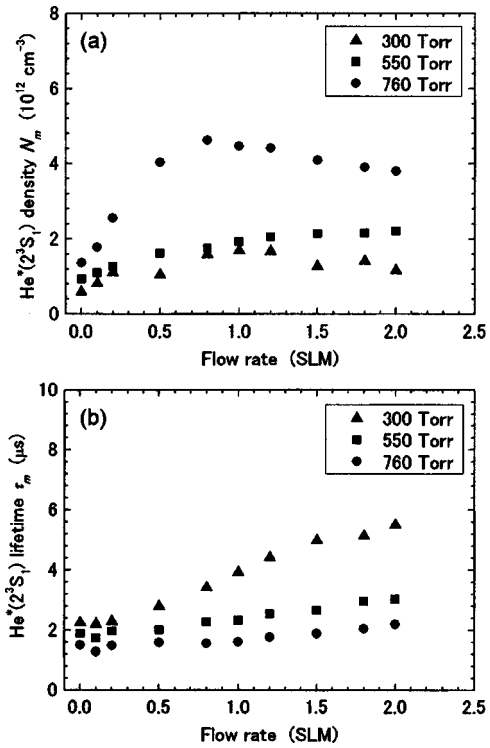

FIG. 5. (a) Density of $He^*(2^3S_1)$ atoms and (b) their lifetime in the afterglow measured in the mesh-electrode system as a function of the gas flow rate at three different pressures.

(after the discharge had been turned off). As the results in Fig. 4(b) indicate, the lifetime $\tau_m(=1/\gamma_m)$ increases with the gas flow rate and then saturates. If we assume the infinite purity of He gas and τ_m is simply determined by the three-body collision process, $He^*+2He \rightarrow He_2^*+He$, and take a published value for the rate constant K_3 as 2.5×10^{-34} cm^6 s^{-1},[16] the estimated values of τ_m become 42.8, 12.7, and 6.7 μs for 300, 550, and 760 Torr at 300 K, respectively. Therefore, the discrepancy between the experimental values must be attributed to the loss of metastable atoms by the Penning-ionization process since the effect of diffusion loss is estimated to be small. If we assume that the dominant impurity is due to the residual N_2 molecules and take a published value for the rate constant of the Penning process K_P as 7×10^{-11} cm^{-3} s^{-1},[17] the estimated impurity level should be about 100 ppm at a flow rate of 1 SLM. Since we are using a conventional grade He gas with nominal purity of 99.99% and a vacuum chamber pumped only by a roughing pump, the suggested impurity level seems reasonable. If we could extrapolate the data of $He^*(2^3S_1)$ density plotted against τ_m to the hypothetical value of 6.7 μs corresponding to the infinite purity, the density might reach 1.5×10^{12} cm^{-3} for the data at 1 atm.

C. Metastable density in the mesh-type system

Similar data measured in the mesh-type system are shown in Figs. 5(a) and 5(b). The values of V_P at 300, 550, and 760 Torr were 0.66, 0.85, and 1.05 kV, respectively. Those data were measured along the path through the mesh, and the absorption length L was assumed to be 1.5 mm according to the results of the other measurement for spatial

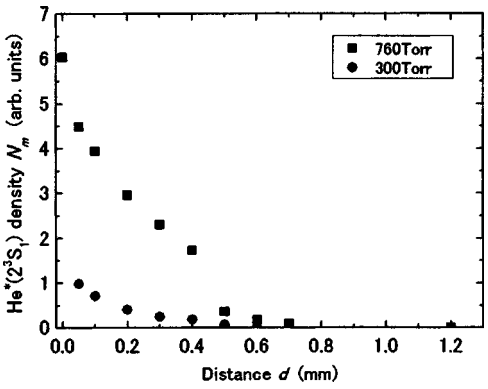

FIG. 6. Spatial distribution of $He^*(2^3S_1)$ density measured in the parallel-plate system at two different pressures as a function of the distance from the electrode surface.

distribution given below. The figures indicate that the density increases with the gas flow and then saturates as seen in the parallel-plate system; however, at atmospheric pressure the density rather starts to decrease at higher flow rates, although a slight tendency to increase remains in the lifetime. In the mesh-type system the active discharge length was about 0.8 mm and the gas flow was conducted through the mesh structure. Therefore, the reason for such an effect could be attributed to the phenomenon that a higher flow tends to blow out the excited species, especially the long-lived metastable atoms, within each period, causing a decrease in the discharge current with the gas flow. The absolute values of the metastable density in the mesh-type system are larger than those in the parallel-plate system by about a factor of five when the total input power in both cases is kept at the same level. Since in the parallel-plate system the active volume of the discharge is larger due to the larger electrode gap, the net input power per volume becomes smaller. A further argument will be given below based on the measurement of the electron density.

The values of τ_m in the mesh-type system are relatively smaller than those in the parallel-plate system. For example, τ_m is about 2 μs in the former case as compared to the value of 4 μs in the latter case at 1 atm. This may be due to the smallness of the discharge space, higher gas flow speed, higher electron density (see below), and so on, which can cause the larger losses of metastable atoms.

The results measured with the laser beam set parallel to the mesh electrode are shown in Fig. 6 as a function of the distance d from the electrode surface. It is clear that the density decreases rapidly with distance within $d=0.2$–0.5 mm, depending slightly on the pressure. The geometrical thickness of the electrode assembly was 1.1 mm [see Fig. 1(b)], so that with the addition of 2×0.2-mm thickness on both sides it might be reasonable to assume the effective absorption length in the case of perpendicular beam configuration to be 1.5 mm.

D. Electron density in both systems

The electron density n_e was derived from the calculated millimeter-wave transmittance characteristics in the procedure mentioned above.[13,14] The decay rate of n_e defined here

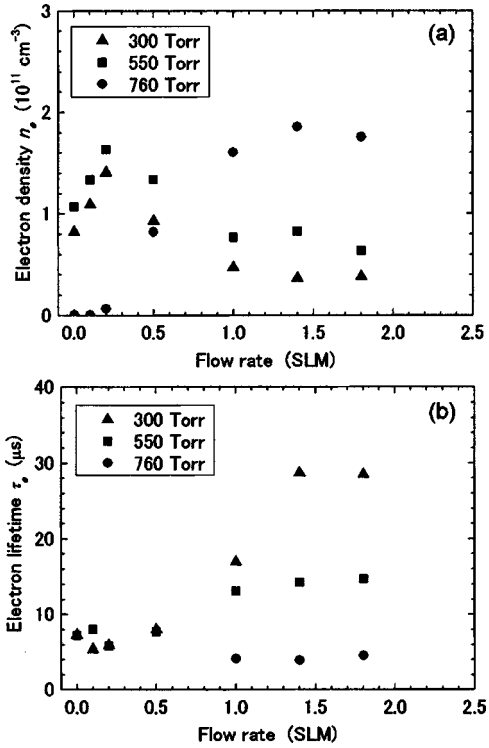

FIG. 7. (a) Electron density and (b) its lifetime in the afterglow measured in the parallel-plate system as a function of the gas flow rate at three different pressures.

as τ_e was also derived from the slope of n_e on a logarithmic plot in the afterglow period. Figures 7(a) and 7(b), respectively, show the data of n_e and τ_e measured in the parallel-plate system as a function of the gas flow rate. In this case, at 1 atm n_e and τ_e behave similarly to the $He^*(2^3S_1)$ density N_m and the lifetime τ_m, respectively, while noticeable differences are seen at lower pressures. The different behaviors between N_m and n_e may be attributed to the change in the contribution of the Penning-ionization process to the production of electrons dependent on the impurity level, which generally becomes larger at lower flow rates. We cannot explain the fairly large values of τ_e as compared to τ_m at lower pressures at the moment. However, the reliability of those data derived from smaller attenuation signals at smaller electron density situations would be lower; the wrong estimation of zero level might artificially yield larger decay constants.

At atmospheric pressure, a comparison of wave forms of the millimeter transmission and the LAS signal shown in Fig. 2(a) for n_e and N_m suggests that in the early period of the rising current the direct ionization process is predominant where a larger peak of n_e appears, while in the afterglow the contribution of Penning ionization becomes important, since both wave forms become similar.

The results measured in the mesh-type system at 1 atm are shown in Fig. 8 for n_e and τ_e, where the values of n_e are taken from the second peak at the negative pulse phase while those for τ_e are obtained from the decay of the third (last) peak. It is seen that n_e increases with the gas flow rate and then saturates similarly to the density of $He^*(2^3S_1)$ atoms. The behavior of τ_e, however, is somewhat different, showing a larger increasing tendency at higher flow rates. The reason

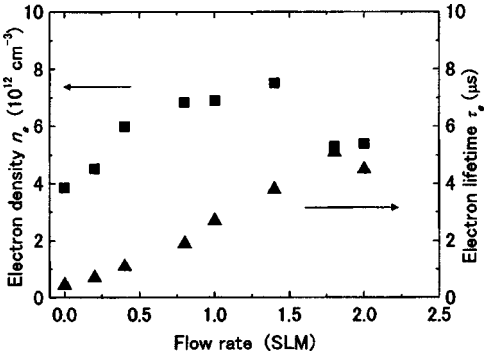

FIG. 8. Electron density and lifetime in the afterglow measured in the mesh-electrode system as a function of the gas flow rate at atmospheric pressure.

for this behavior is not clear as above except the artificial errors due to smaller signals. When we switched the discharge gas from He to Ar in the same situation, the rise and decay of millimeter-transmittance signal become faster, suggesting the no contribution of the Penning process of metastable Ar atoms for the production of electrons. The shorter τ_e in Ar also suggests the decay of electrons due to the recombination loss is faster than that of the metastable atoms. Therefore, the longer decay of n_e observed in He could be attributed to the production by the Penning process of $He^*(2^3S_1)$ atoms.

IV. DISCUSSION

By using the LAS method, the density of $He^*(2^3S_1)$ atoms has been measured successfully in DBD plasmas under the atmospheric pressure condition. The method's accuracy is very good in itself for the average density, although it is not effective for deriving the spatial distributions along the line of sight. Especially in the present case of the mesh-type discharge, the produced plasma is not uniform along the axis of a hole. Therefore, in practice we had to take an effective absorption length to be about the thickness of the electrode assembly. In a coplanar-type surface discharge, the density distribution may have a complicated spatial distribution such as in unit cell of an ac-type plasma display panel, which we have previously measured.[18,19] Nevertheless, the total number of metastable atoms integrated along the measured path obtained directly by the LAS method is accurate and useful for estimating the overall production efficiency of $He^*(2^3S_1)$ atoms per input power. On the other hand, in the case of the parallel-plate system, the distribution along the line of sight is quite uniform, while the perpendicular distribution between the electrodes is not. The laser beam diameter used here was fairly large almost covering the entire gas gap, so that the spatially resolved measurement across the gap was impossible. We would like to leave those measurements for a future work.

As for the millimeter-wave transmission measurement of n_e, the accuracy is much lower due to the complicated nature of the transmission modes through the present electrode assemblies. As the first approximation, we had to take the simplest assumption of uniform slab structures. In addition, the spatially resolved measurements were impossible with this method. Therefore, the absolute values derived here should

be understood as only order estimations. However, it has turned out that this method is very effective for the measurements of n_e in the temporal behaviors. Actually, the importance of the metastable atoms for the production of electrons by the Penning process has been clarified experimentally by this method, for the first time, in atmospheric pressure plasmas.

Here, we would like to compare the characteristics between the two experimental systems. The measured density of $He^*(2^3S_1)$ atoms in the mesh-type system is about five times higher than that in the parallel-plate system as Figs. 3 and 4 show. As for n_e, it differs in those systems by about one order of magnitude as seen from Figs. 7 and 8. Those results are mainly attributed to the difference in the input power density per unit volume. In the parallel-plate system the electrode gap is 3 mm, while in the mesh-type system it is roughly 1 mm, although accurate identification is difficult. In a comparison of the volume of active discharge space, it is estimated to be 5.4 cm^3 in the former and 0.5 cm^3 in the latter. Therefore, when we keep the input power in the same order, the power density can differ by almost an entire order of magnitude. This means that the electrical efficiency for the production of metastable atoms and electrons differs little in those systems; the major difference is rather in their geometrical characteristics, i.e., larger volume with low density in the former and larger density with smaller volume in the latter. Thus, proper choices of the characteristics for specific applications are important according to the circumstances.

We found only one previous publication on the measurement of $He^*(2^3S_1)$ atoms in atmospheric pressure DBD plasma, where a laser-induced collisional fluorescence (LICF) method was used.[20] However, the absorption measurement at 389-nm transition tried there at the same time was unsuccessful due to too small signals. The density derived from the absolute calibration of the LICF signal through analysis with rate equations is about 1.5×10^{10} cm^{-3} at 1 atm, which is an order of magnitude smaller than our result in the similar parallel-plate system. This might be due to the difference in the impurity levels. Actually, in the measured temporal behavior of the $He^*(2^3S_1)$ density by Nersiayan *et al.*, the decay almost follows the discharge current in contrast to our results that show much longer decay. Thus, the impurity concentration in their case might be around the 10^3-ppm level.

There are a few previous reports on the APGD in He,[7,21–23] especially on the contribution of the Penning ionization of impurities.[7,23] These reports employ theoretical approaches using one-dimensional fluid models. It is commonly mentioned that in the earlier period of the current-rise phase the direct ionization of He atoms is the major process, but in the later period of the afterglow phase the Penning-ionization process becomes predominant. The effect of the Penning ionization remains until the next discharge phase, so that it can produce seed electrons necessary for maintaining uniform glow discharge. This argument is consistent with our present experimental results. Although the contribution depends heavily on the impurity level, it is conventionally between 10 and 1000 ppm, thereby validating the explanation. In Ref. 23 the absolute values of N_m and n_e are given as

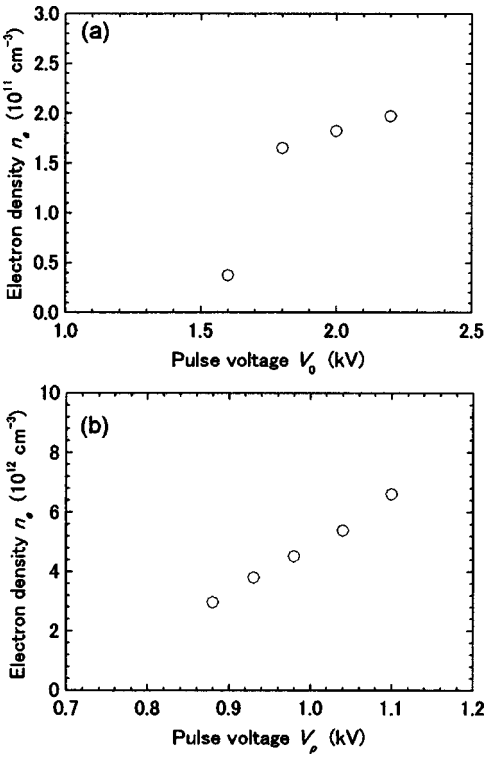

FIG. 9. The variation of electron densities with applied voltages measured in (a) parallel-plate and (b) mesh-electrode systems at a gas flow rate of 2 SLM.

3.4×10^{10} and 2.5×10^{10} cm^{-3}, respectively, at the spatiotemporal peak and at the impurity level of 100 ppm in a similar situation. Those are about one order of magnitude smaller than our measured results given in Figs. 4(a) and 7(a) at 1 atm. However, values of N_m and n_e are dependent on the input power as shown in Figs. 9(a) and 9(b), which have been measured, respectively, in the parallel-plate system and the mesh-type systems by changing the applied pulse voltages. (In Fig. 9(a) $V_0=1.6$ kV is close to the minimum sustain voltage, so that n_e drops rapidly.) Thus, for more quantitative comparisons, we have to specify the differences in the conditions of experiments and simulations as well as to perform the spatially resolved measurement as mentioned above.

V. CONCLUSIONS

The absolute density of $He^*(2^3S_1)$ metastable atoms were measured, for the first time, by a LAS method at the 1083-nm line in two different types of DBD at atmospheric pressure. The peak values in the parallel-plate system were in the order of 10^{11} cm^{-3}, while those in the mesh-type system are larger by about a factor of five, although the results are strongly dependent on the gas flow rate. The electron density n_e was also estimated from a millimeter-wave transmission method in the 50–75 GHz range, giving results in the order of 10^{11} cm^{-3} in the parallel-plate system and 10^{12} cm^{-3} in the mesh-type system, respectively. Those temporal behaviors verified the importance of the Penning-ionization process for producing electrons in the afterglow phase, although the contribution strongly depends on the impurity level.

ACKNOWLEDGMENTS

This work is partially supported by the Grants-in-Aid for Scientific Research on Priority Area of Microplasmas from the Japanese Ministry of Education, Culture, Sports, Science and Technology.

[1]E. E. Kunhardt, IEEE Trans. Plasma Sci. **28**, 189 (2000).
[2]U. Kogelschatz, Plasma Chem. Plasma Process. **23**, 1 (2003).
[3]*Non-Equilibrium Air Plasmas at Atmospheric Pressure*, edited by K. H. Becker, U. Kogelschatz, K. H. Schoenbach, and R. J. Barker (IOP, Bristol, 2005).
[4]S. Kanazawa, M. Kogoma, T. Moriwaki, and S. Okazaki, J. Phys. D **21**, 838 (1988).
[5]S. Okazaki, M. Kogoma, M. Uehara, and Y. Kimura, J. Phys. D **26**, 889 (1993).
[6]N. Gherardi and F. Massines, IEEE Trans. Plasma Sci. **29**, 536 (2001).
[7]F. Massines, P. Segur, N. Gherardi, C. Khamphan, and A. Ricard, Surf. Coat. Technol. **174–175**, 8 (2003).
[8]Yu. B. Golubovskii, V. A. Maiorov, J. Behnke, and J. F. Behnke, J. Phys. D **36**, 975 (2003).
[9]Yu. B. Golubovskii, V. A. Maiorov, J. F. Behnke, J. Tepper, and M. Lindmayer, J. Phys. D **37**, 1346 (2004).
[10]T. Somekawa, T. Shirafuji, O. Sakai, and K. Tachibana, J. Phys. D **38** (2005) (in press).
[11]O. Sakai, Y. Kishimoto, and K. Tachibana, J. Phys. D **38**, 431 (2005).
[12]M. W. Millard, P. P. Yaney, B. N. Ganguly and C. A. DeJoseph, Jr., Plasma Sources Sci. Technol. **7**, 389 (1998).
[13]K. Tachibana, Y. Kishimoto, S. Kawai, T. Sakaguchi, and O. Sakai, Plasma Phys. Controlled Fusion **47**, A167 (2005).
[14]J. D. Swift and M. J. R. Schwar, *Electrical Probes for Plasma Diagnostics* (IIiffe, London, 1970), p. 286.
[15]D. Vrinceanu, S. Kotochigova, and H. R. Sadeghpour, Phys. Rev. A **69**, 022714 (2004).
[16]A. V. Phelps, Phys. Rev. **99**, 1307 (1955).
[17]R. S. F. Chang, D. W. Setser, and G. W. Taylor, Chem. Phys. **35**, 201 (1978).
[18]K. Tachibana, K. Mizokami, N. Kosugi, and T. Sakai, IEEE Trans. Plasma Sci. **31**, 68 (2003).
[19]Y. Shintani, J.-C. Ahn, K. Tachibana, T. Sakai, and N. Kosugi, J. Phys. D **36**, 2928 (2003).
[20]G. Nersiayan, T. Morrow, and W. G. Graham, Appl. Phys. Lett. **85**, 1487 (2004).
[21]F. Tochikubo, T. Chiba, and T. Watanabe, Jpn. J. Appl. Phys., Part 1 **38**, 5244 (1999).
[22]X. Yuan and L. L. Raja, Appl. Phys. Lett. **81**, 814 (2002).
[23]L. Mangolini, C. Anderson, J. Heberlein, and U. Kortshagen, J. Phys. D **37**, 1021 (2004).